Chapter 7

Hydrogenation of Zr-Based Quasicrystals

Devinder Singh, Radhey Shyam Tiwari and
Onkar Nath Srivastava

Additional information is available at the end of the chapter

http://dx.doi.org/10.5772/66255

Abstract

In this chapter, results of our recent investigations on the hydrogenation behavior of Zr-based quasicrystalline alloys and its effect on their structural and microhardness behavior have been discussed. The microstructural changes with respect to the addition of Ti and their correlation with hydrogen storage characteristics of $(Zr_{69.5}Al_{7.5}Cu_{12}Ni_{11})_{100-x}Ti_x$ (x = 0, 4 and 12) quasicrystalline alloys have been studied. The substitution of Ti affects the nucleation and growth characteristics of nano-quasicrystals. The grain size of quasicrystals decreases with addition of Ti. The hydrogen uptake capacity of partially quasicrystalline alloys has been improved by the addition of Ti. The alloys with x = 0, 4, and 12 absorbed 1.20 wt.%, 1.38 wt.%, and 1.56 wt.% of hydrogen, respectively. A significant effect on the structure/microstructure and mechanical behavior of $(Zr_{69.5}Al_{7.5}Cu_{12}Ni_{11})_{100-x}Ti_x$ quasicrystalline alloys due to hydrogenation has been observed. The change in the microhardness behavior has been discussed based on microstructural variation resulting to Ti addition. The study is focused on investigations of these materials to understand the structure (microstructure)-property correlations.

Keywords: hydrogenation, quasicrystalline, composites, microstructure, microhardness

1. Introduction

Storage is an important issue with hydrogen to become a renewable, clean, and climate friendly fuel. The chemical interactions between the metal and hydrogen atoms, number, type, and size of the interstitial sites for hydrogen mainly determine the storage capacity of hydrogen in metals and alloys. Metals and alloys based on transition metals are the most common materials for hydrogen storage. Hydrogen tends to occupy tetrahedral interstitial sites in these materials.

Quasicrystals have been found to exhibit certain important characteristic properties like high hardness, high oxidation resistance, low surface energy, and low thermal conductivity which make these materials attractive for technological applications [1–7]. These materials have received considerable attention as hydrogen storage materials after the discovery of thermodynamically stable icosahedral quasicrystalline phase in Ti-based alloys [8, 9]. Due to the presence of high density of interstitial voids in quasicrystalline alloys, these materials have shown to reversibly store a large amount of hydrogen. The storage capacity can reach up to 3 wt.% of hydrogen [10]. This may be better than that of the crystalline La-based, V-based, and Fe-Ti hydrogen storage alloys [11–13]. Ti- and Zr-based quasicrystalline alloys have a large number of tetrahedral coordinated sites. The Zr-Al-Cu-Ni quasicrystalline alloy is a promising material for the hydrogen storage applications due to the presence of local tetrahedral order and favorable chemical composition [14–17]. The metallic glasses and their composites are known to absorb hydrogen during electrochemical charging, up to a hydrogen per metal atom content (H/M) of 1.6 for the quasicrystalline phase [18, 19] and H/M = 1.0 for the glassy phase [20, 21], respectively. A similar hydrogen uptake from the gas phase is needed with no irreversible phase transformation in order to use these materials for hydrogen storage. It has been found that the hydrogen storage capacity is higher, and the absorption kinetics is faster for the quasicrystalline phase than for the glassy phase [15, 18, 21]. The presence of a large number of tetrahedral sites assumed for icosahedral structure has led to enhanced hydrogen storage capacity. Thus, it is relevant to study the hydrogenation characteristics of quasicrystalline phase. Though Zr-based and Ti-based quasicrystals are among the best in the group of hydrogen storage alloy systems [17, 22–26], still there are issues in regard to their structural stability with hydrogenation. The icosahedral phase (I-phase) in $Zr_{69.5}Al_{7.5}Cu_{12}Ni_{11}$ alloy is metastable. When the $Zr_{69.5}Al_{7.5}Cu_{12}Ni_{11}$ alloy is annealed for a longer time, the metastable I-phase decomposes into crystalline phases [27–31]. Hence, the hydrogen storage capacity will be deteriorated due to the lack of significant polytetrahedral order in these crystalline phases. The desorption of hydrogen was not observed to ensue at temperatures less than about 450°C, most likely due to thin oxide layers formed at the surfaces of the partially quasicrystalline $Zr_{69.5}Al_{7.5}Cu_{12}Ni_{11}$ ribbons [16]. During annealing at higher temperatures, the I-phase decomposed by a discontinuous transformation into tetragonal Zr_2Cu, tetragonal Zr_2Ni, and hexagonal Zr_6NiAl_2 starting with a precipitation reaction of Zr_2Cu [32–34]. In view of application, there are still major concerns regarding the effect of hydrogenation on the structure of these quasicrystalline alloys and consequently its influence on the mechanical properties. Thus, the study of hydrogenation effect on the structure/microstructure and mechanical behavior of $Zr_{69.5}Al_{7.5}Cu_{12}Ni_{11}$ quasicrystalline alloy is of special interest.

2. Investigation of nominal composition: $Zr_{69.5}Al_{7.5}Cu_{12}Ni_{11}$

The $Zr_{69.5}Al_{7.5}Cu_{12}Ni_{11}$ alloy with a thickness of ~40–50 μm and lengths of ~1–2 m has been synthesized using melt-spinning technique [23, 35]. During melt spinning the entire apparatus was enclosed in a steel enclosure through which argon gas was continuously flowing. This was done to prevent oxidation of the ribbons after ejection of melt from the nozzle. For annealing

http://dx.doi.org/10.5772/66255

experiments, the ribbons were packed in a Ta foil and then sealed in a silica ampoule under an argon atmosphere. The ribbons were isothermally annealed in vacuum (10^{-6} Torr) using a Heraeus furnace with temperature control of ±1°C.

For exploring the gross structural feature, X-ray diffraction (XRD) studies of the as-formed ribbons were done. **Figure 1a** shows the representative XRD pattern of the $Zr_{69.5}Al_{7.5}Cu_{12}Ni_{11}$ as-synthesized ribbon. As can be seen, the XRD pattern shows two broad halos. This shows that the as-formed material is amorphous (glassy). However, for the as-synthesized ribbon (c.f. **Figure 1a**), broad halo within the angular range of 30–45° followed by another weaker second broad halo within the angular range of 60–70° is seen. The material was then annealed in the anticipation that the synthesized amorphous phase will transform to the quasicrystalline/crystalline version. In order to estimate the transformation temperature, differential scanning calorimetry (DSC) technique was employed. **Figure 1b** shows the constant-rate heating DSC scan (20 K/min) of the melt-spun $Zr_{69.5}Al_{7.5}Cu_{12}Ni_{11}$ alloy. Heating the melt-spun ribbon from room temperature up to elevated temperatures reveals a distinct endothermic event characteristic of the glass transition (T_g) at 624 K. With increasing temperature the DSC curve exhibits two peaks (T_{p1} and T_{p2}) with onset temperatures T_{x1} and T_{x2} (702 K and 727 K, respectively). The supercooled liquid region, defined as $\Delta T_x = T_{x1} - T_g$ corresponds to the stability of the supercooled liquid against crystallization and is found to be 78 K. The melting temperature (T_m) of the melt-spun $Zr_{69.5}Al_{7.5}Cu_{12}Ni_{11}$ is found to be 1064 K. The first peak (T_{p1}) results from the quasicrystal (qc) formation. The second peak (T_{p2}) corresponds to the decomposition of quasicrystals as well as the transformation of the remaining amorphous matrix into a crystalline phase.

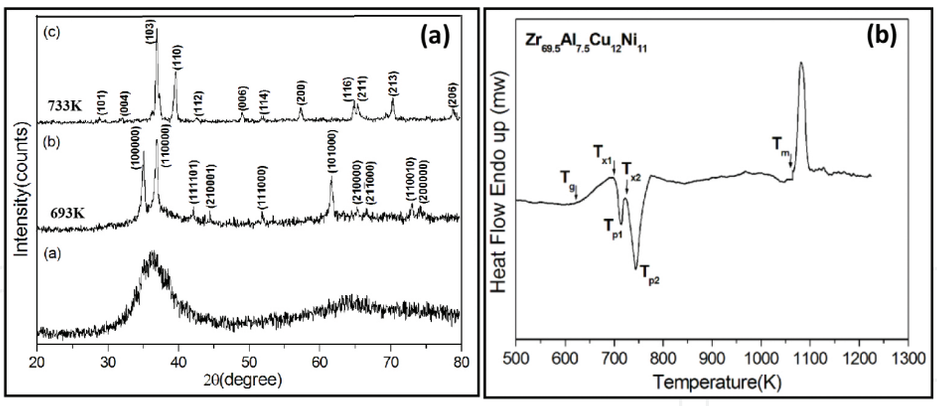

Figure 1. (a) XRD patterns of as-synthesized and annealed ribbons of $Zr_{69.5}Al_{7.5}Cu_{12}Ni_{11}$ alloy at 693 K and 733 K for 15 min and (b) DSC curve of the melt-spun $Zr_{69.5}Al_{7.5}Cu_{12}Ni_{11}$ alloy at the heating rate of 20 K/min.

The XRD patterns of the melt-spun ribbons (**Figure 1a**) exhibit the typical broad diffuse maxima characteristic of amorphous materials and no traces of crystalline phases. When the sample is isothermally heated at 693 K (i.e., near T_{x1}) for 15 min, the XRD pattern displays diffraction peaks with positions and intensity ratios that are typical for powder diffraction patterns of quasicrystals. The reflections can be indexed to I-phase. One can notice the broad overlapping diffraction peak due to amorphous phase in addition to the quasicrystalline diffraction peaks

in the annealed XRD patterns. This indicates that during the first devitrification step, the phase transformation from glass to quasicrystalline is not complete and a residual glassy phase retained in the sample. This suggests that quasicrystal formation is a primary transformation. As evident from **Figure 1a**, heating the ribbon to 733 K (i.e., near T_{x2}) leads to the formation of a tetragonal Zr_2Cu-type phase (space group I4/mmm (139), a = 3.218 Å, c = 11.180 Å). No trace of quasicrystals is detected at this stage of crystallization, indicating that the quasicrystalline phase is metastable and transforms into more stable crystalline phase.

The $Zr_{69.5}Al_{7.5}Cu_{12}Ni_{11}$ melt-spun ribbon was observed to be fully amorphous by means of transmission electron microscopy (TEM). **Figure 2a** and the inset show the TEM micrograph and corresponding selected area electron diffraction (SAED) pattern displaying diffuse halos for $Zr_{69.5}Al_{7.5}Cu_{12}Ni_{11}$ alloy. The presence of two halos is suggestive of the presence of short-range order with two different correlation lengths. The TEM bright-field micrograph displaying no discernible contrast indicates the formation of glassy phase in the system. **Figure 2b** shows the typical microstructure of a partially transformed $Zr_{69.5}Al_{7.5}Cu_{12}Ni_{11}$ ribbon with spherical quasicrystals. The inset of **Figure 2b** shows the fivefold diffraction pattern of the quasicrystalline phase. Since no diffraction patterns corresponding to the other crystalline structure are seen, the initial precipitation phase in $Zr_{69.5}Al_{7.5}Cu_{12}Ni_{11}$ alloy is only quasicrystalline phase.

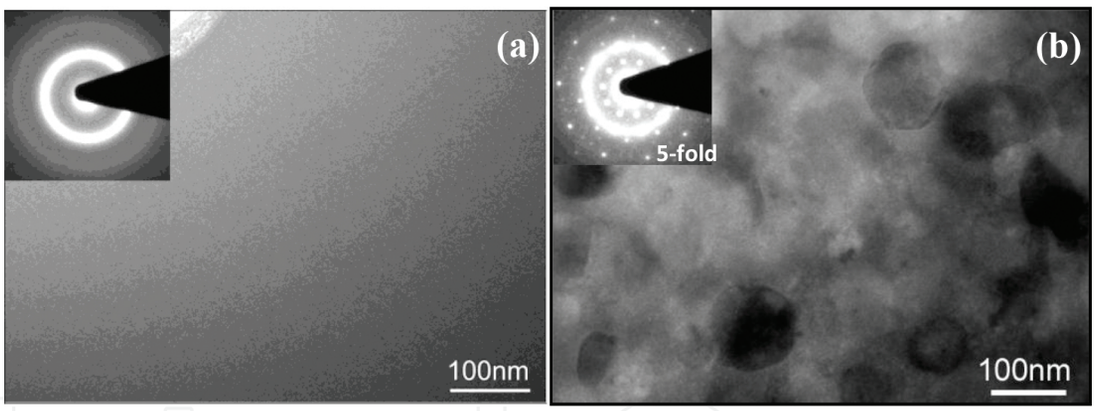

Figure 2. (a) TEM image and the corresponding diffraction pattern of as-synthesized $Zr_{69.5}Al_{7.5}Cu_{12}Ni_{11}$ alloy. (b) TEM microstructure of $Zr_{69.5}Al_{7.5}Cu_{12}Ni_{11}$ alloy showing the presence of spherical quasicrystals. Inset of (b) shows the SAED pattern of the quasicrystalline (qc) phase along the fivefold direction.

3. Effect of material tailoring on the hydrogen storage properties

The structure and phase formation of Zr-Al-Cu-Ni alloy system is strongly affected by material tailoring. Several studies reveal that the compositional changes may influence the hydrogen storage capacity of Zr-based alloys [19–21]. In the present chapter, the effect of Ti addition on the phase formation and the hydrogen storage characteristics of $(Zr_{69.5}Al_{7.5}Cu_{12}Ni_{11})_{100-x}Ti_x$ alloys with $0 \leq x \leq 12$ have been discussed. The influence of hydrogenation from the gas phase on the structure/microstructure and microhardness behavior of these melt-spun quasicrystal-

http://dx.doi.org/10.5772/66255

line alloys have been studied. The present study deals with the synthesis, phase formation, change in the microstructure with respect to Ti addition, and their correlation with hydrogen storage characteristics of Zr-Al-Cu-Ni alloys.

3.1. Microstructural and structural features

Figure 3a shows the XRD patterns of as-synthesized $(Zr_{69.5}Al_{7.5}Cu_{12}Ni_{11})_{100-x}Ti_x$ (x = 0, 4, 12 at. %) melt-spun alloys. It can be seen that all the patterns of the alloys consist of only broad diffraction maxima without a detectable sharp Bragg peak, indicating that the samples are amorphous in nature. The TEM image and its corresponding SAED pattern displaying diffuse halos for the alloy with x = 12 is shown in **Figure 3b**. The TEM microstructure for the samples with x = 12 or less displays a featureless contrast, which is the typical appearance of an amorphous phase. The DSC scans for the samples recorded at a heating rate of 20 K/min are shown in **Figure 4**. **Table 1** gives the thermal stability data for all the investigated samples. With increasing Ti content, the onset crystallization temperature (T_x) decreases gradually, whereas the change of glass transition temperature (T_g) is very subtle. The crystallization for the alloys with x = 0–12 follows a two-step process.

The primary crystallization products of these melt-spun alloys were examined after isothermal annealing. **Figure 5** compares XRD patterns for partially crystallized ribbons with x = 0, 4, and 12. Isothermal annealing of these samples was carried out for 15 min at 425°C (for x = 0 and 4) and 420°C (for x = 12). The respective annealing temperatures for these alloys have been found through DSC investigation (c.f. **Table 1**). The crystallization processes of alloys with x = 0–12 show the formation of quasicrystalline phase. The indexing of the Bragg peaks in the XRD patterns was done on the basis of I-phase [36, 37]. For the alloy with x = 12, the XRD pattern shows considerable peak broadening as compared to the alloys with x = 0 and 4. This is for the reason that the size of the precipitates is decreasing with increasing Ti content. The quasicrystalline-phase formation in these samples was further investigated by TEM. The nanometer-sized quasicrystalline grains of the annealed samples for the alloys with x = 0, 4, and 12 are shown in **Figure 6a–c**. The grain size of quasicrystals decreases with addition of Ti. The quasicrystal grains with average size of ~125 nm and ~80 nm have been observed for the alloys with x = 0 and 4, respectively. The presence of characteristic fivefold icosahedral symmetry can be seen in the corresponding SAED pattern. The alloy with x = 12 reveals the formation of 5–10 nm grains. Thus, the strong reduction in the grain size has been observed for this alloy. The corresponding SAED pattern for the alloy with x = 12 shows the presence of diffraction rings (inset in **Figure 6c**) indexed with I-phase. The diffraction patterns with diffuse ring confirm the presence of a residual glassy phase after the first devitrification step. These results show that the size of the quasicrystalline grains decreases with addition of Ti in $(Zr_{69.5}Al_{7.5}Cu_{12}Ni_{11})_{100-x}Ti_x$ alloys. The nucleation rate of the I-phase increases with increase in the concentration of Ti. Thus, in the present case, it can be said that the addition of Ti affects the nucleation and growth characteristics of quasicrystals significantly.

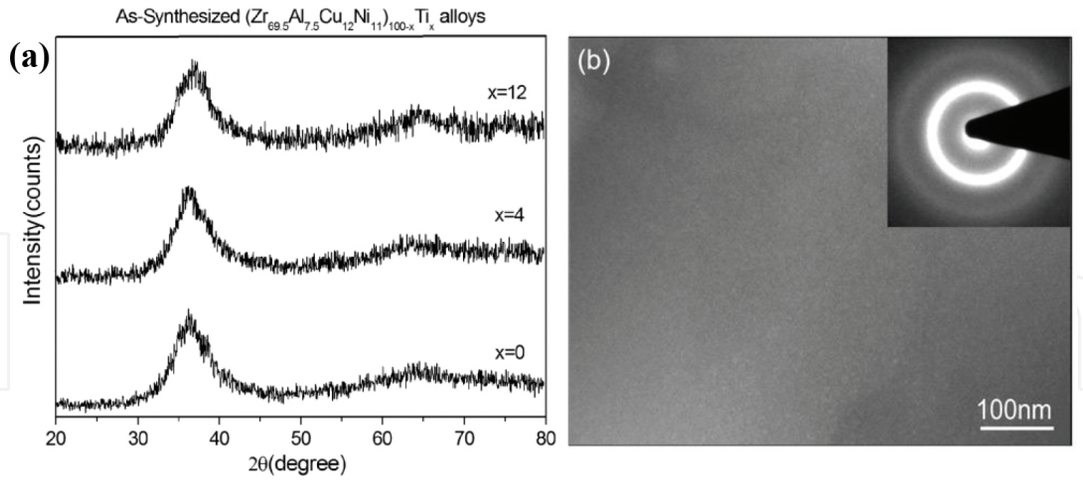

Figure 3. (a) XRD patterns of as-synthesized ribbons of $(Zr_{69.5}Al_{7.5}Cu_{12}Ni_{11})_{100-x}Ti_x$ alloys. (b) TEM image and the corresponding diffraction pattern of as-synthesized $(Zr_{69.5}Al_{7.5}Cu_{12}Ni_{11})_{88}Ti_{12}$ alloy (reprinted with kind permission from Ref. [23], Copyright 2013, Elsevier).

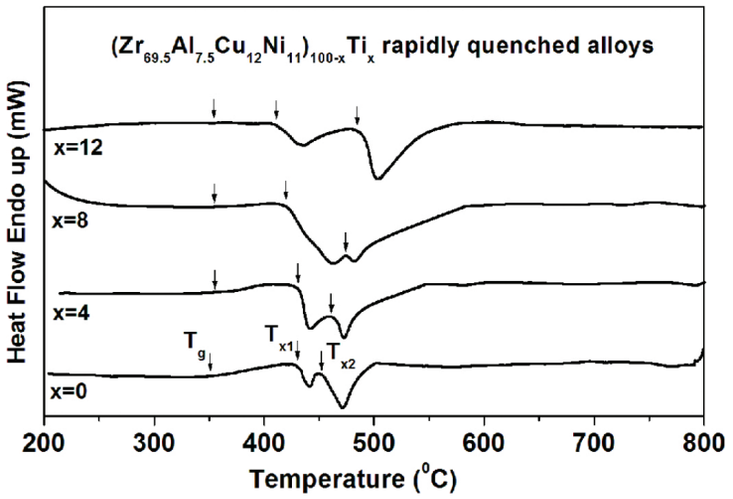

Figure 4. DSC curves of the melt-spun $(Zr_{69.5}Al_{7.5}Cu_{12}Ni_{11})_{100-x}Ti_x$ alloys [35].

x (at.%)	T_g (°C)	T_{x1} (°C)	T_{x2} (°C)	ΔT_x (°C)
0	351	429	453	78
4	355	429	461	74
8	355	420	474	65
12	355	413	480	58

T_g: glass transition temperature; T_{x1}: first-onset crystallization temperature; T_{x2}: second-onset crystallization temperature; ΔT_x: supercooled liquid region

Table 1. Thermal analysis of the melt-spun $(Zr_{69.5}Al_{7.5}Cu_{12}Ni_{11})_{100-x}Ti_x$ ribbons [35].

http://dx.doi.org/10.5772/66255

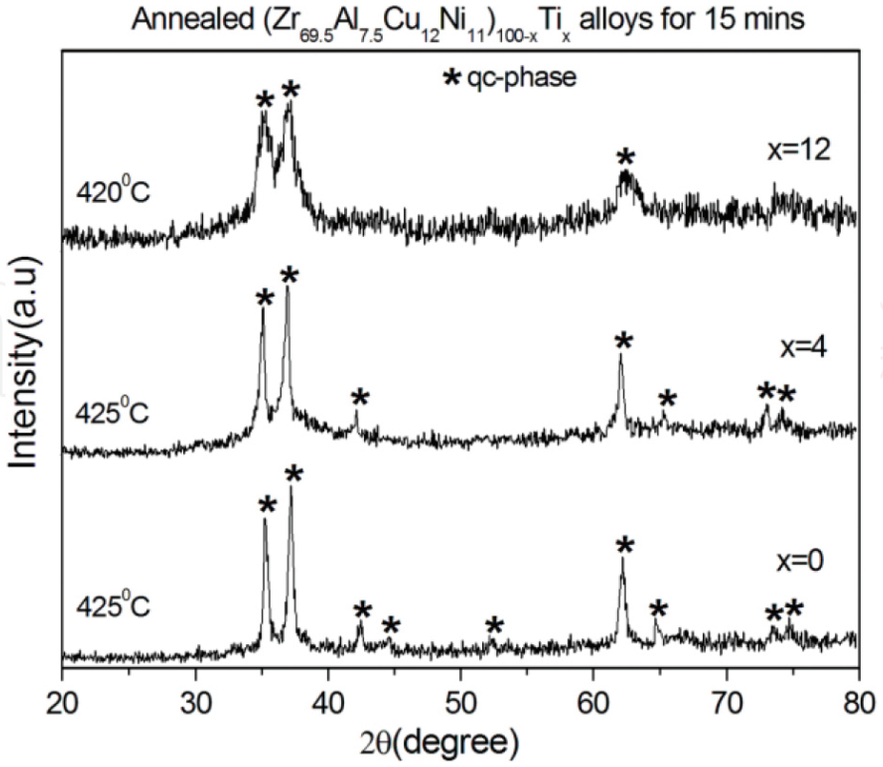

Figure 5. XRD patterns of annealed ribbons of $(Zr_{69.5}Al_{7.5}Cu_{12}Ni_{11})_{100-x}Ti_x$ alloys (reprinted with kind permission from Ref. [23], Copyright 2013, Elsevier).

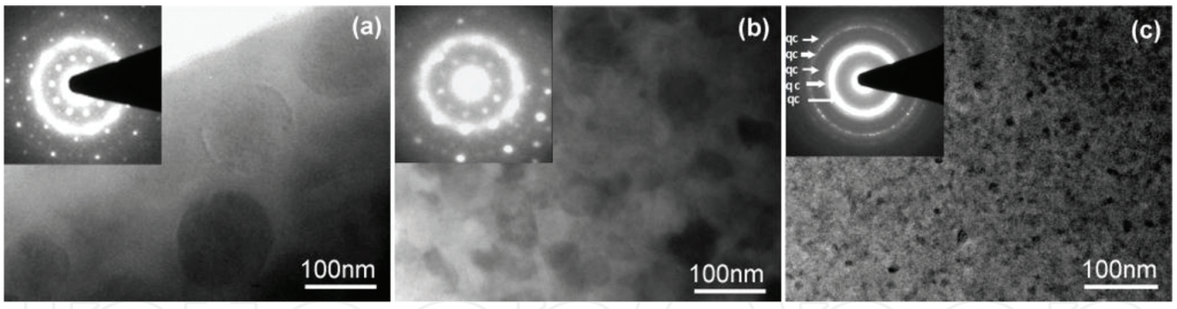

Figure 6. Bright-field TEM images of $(Zr_{69.5}Al_{7.5}Cu_{12}Ni_{11})_{100-x}Ti_x$ alloys (a) x = 0, (b) x = 4, and (c) x = 12 showing the influence of the Ti content on size of the quasicrystalline phase (reprinted with kind permission from Ref. [23], Copyright 2013, Elsevier).

A quantitative energy-dispersive X-ray (EDX) analysis was employed for the composition determination. **Figure 7a–c** shows EDX spectra of the $(Zr_{69.5}Al_{7.5}Cu_{12}Ni_{11})_{100-x}Ti_x$ alloys with x = 0, 4, and 12, respectively. **Table 2** presents EDX quantitative analysis along with deviations of the $(Zr_{69.5}Al_{7.5}Cu_{12}Ni_{11})_{100-x}Ti_x$ (x = 0–12) alloys. The semiquantitative analysis of EDX pattern at 3–5 points gives the deviations in the elemental compositions. Based on the EDX quantitative analysis, it has been found that the investigated compositions of the alloys are very close to stoichiometric proportions of nominal compositions. The presence of oxygen within the detectable limit of EDX was not found.

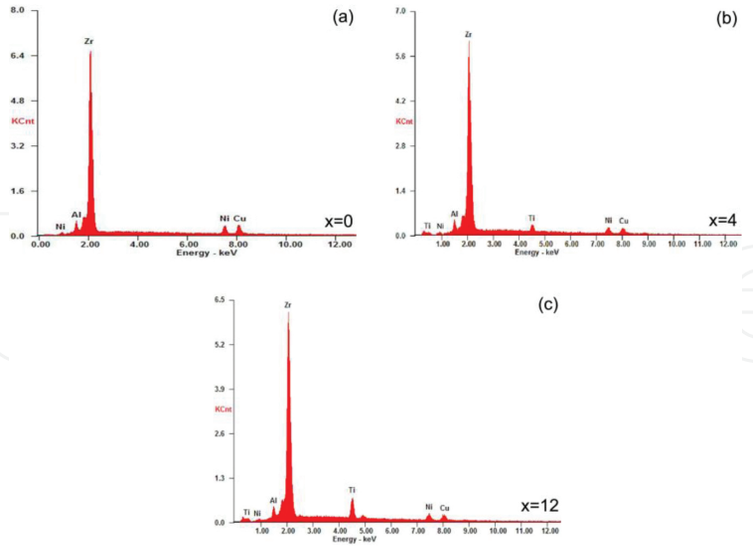

Figure 7. Energy-dispersive spectra of the melt-spun $(Zr_{69.5}Al_{7.5}Cu_{12}Ni_{11})_{100-x}Ti_x$ (x = 0, 4 and 12) alloys.

Alloy composition x (at.%)	Zr (±0.7)	Al (±0.3)	Cu (±0.5)	Ni (±0.5)	Ti (±0.5)
0	68.7	7.3	12.5	11.5	–
4	66.1	6.9	12.2	9.8	5.0
12	60.7	6.5	11.6	8.3	12.9

Table 2. Compositions of the $(Zr_{69.5}Al_{7.5}Cu_{12}Ni_{11})_{100-x}Ti_x$ alloys (in at.%) based on EDX quantitative analysis (reprinted with kind permission from Ref. [23], Copyright 2013, Elsevier).

3.2. Hydrogenation characteristics

In this section, we discuss the results of the hydrogenation characteristics of three glassy composites. The computerized pressure-concentration-temperature (PCT) apparatus supplied by Advance Materials Corporation (USA) has been used to study the hydrogen sorption characteristics of the partially crystallized ribbons. The gas reaction control-based software has been used to monitor the temperature, pressure, and gas desorbed/absorbed through the samples. The estimated error in the hydrogen storage capacity measurement for the alloys is ±0.02 wt.%. Temperature-programmed desorption (TPD) experiments at a heating rate of 5°C/min were also performed in addition to hydrogen sorption behavior. The absorption kinetic experiments were performed at fixed temperature and pressure to study the hydrogen storage characteristics of $(Zr_{69.5}Al_{7.5}Cu_{12}Ni_{11})_{100-x}Ti_x$ (x = 0, 4, and 12) quasicrystal-glass composites. It may be noted that hydrogen storage here is through dissociation of hydrogen molecule into hydrogen atoms. The catalytic activity of surface transition metal atoms is responsible for the dissociation of hydrogen molecule into hydrogen atoms. The dissociation is followed by diffusion of hydrogen atoms in the interstitial sites. Different temperatures and pressures range from 250 to 300°C and 5–10 MPa for 2–3 h have been performed for the hydrogenation experiments. The best results were found with temperature 270°C and 8 MPa of hydrogen

pressure. The hydrogenation for the partially crystallized ribbons was done in a high-pressure reactor. The reactor containing the ribbons was evacuated by a rotary pump (10^{-2} Torr), heated up to 270°C, and then charged with 8 MPa of hydrogen pressure.

The hydrogen absorption characteristics for the alloys with x = 0, 4, and 12 at 270°C temperature and 8 MPa hydrogen pressure are shown in **Figure 8**. The absorption kinetics and hydrogen uptake capacity of the composites increase with increasing concentration of Ti (as shown in **Table 3**). The hydrogen storage capacity for the alloys with x = 0, 4, and 12 is found to be 1.20 wt. %, 1.38 wt.%, and 1.56 wt.%, respectively. The alloy with x = 0 having less hydrogen storage capacity of 1.20 wt.% with 100–150 nm grains whereas the alloy with x = 4 can store 1.38 wt.% of hydrogen with 60–100 nm grains at same conditions of temperature and pressure. The hydrogen storage capacity further increases to 1.56 wt.% for the alloy with x = 12 for grain size in the range 5–10 nm. It may be noted here that the experimental conditions for the synthesis of melt-spun ribbons were identical for all the alloys. In the present case, the enhancement in storage capacity is ~23% over the normal storage capacity of $Zr_{69.5}Al_{7.5}Cu_{12}Ni_{11}$ quasicrystalline phase.

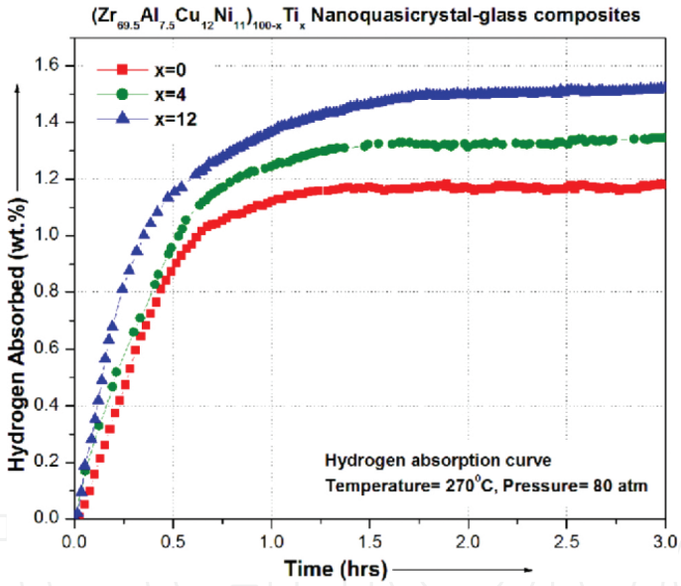

Figure 8. Hydrogen absorption kinetic curves of $(Zr_{69.5}Al_{7.5}Cu_{12}Ni_{11})_{100-x}Ti_x$ (x = 0, 4 and 12) quasicrystal-glass composites (reprinted with kind permission from Ref. [23], Copyright 2013, Elsevier).

Alloy composition	Quasi-lattice parameter		Storage capacity (wt.%) (±0.02)
x (at.%)	Before hydrogenation (a_i^0)	After hydrogenation (a_i^H)	
0	5.108 Å	5.201 Å	1.20
12	5.141 Å	5.293 Å	1.56

Table 3. Hydrogenation characteristics of $(Zr_{69.5}Al_{7.5}Cu_{12}Ni_{11})_{100-x}Ti_x$ (x = 0, 4, and 12) quasicrystal-glass composites (reprinted with kind permission from Ref. [23], Copyright 2013, Elsevier).

The probable reasons for the enhancement in the hydrogen storage capacity of $(Zr_{69.5}Al_{7.5}Cu_{12}Ni_{11})_{100-x}Ti_x$ alloys are: (i) it has been observed by XRD and TEM analysis that the grain refinement occurred with increase in the concentration of Ti. The increase of grain boundary density provides better interaction between hydrogen and I-phase and consequently increases the hydrogen storage uptake capacity. The enhancement in hydrogen storage capacity due to grain refinement has also been reported in Ti-Zr-Ni and Mg-Ni-Mm alloys [22, 38]. (ii) The other probable reason for the increase in hydrogen absorption may also be due to Ti addition. The addition of Ti in $Zr_{69.5}Al_{7.5}Cu_{12}Ni_{11}$ quasicrystalline alloy may have twofold effects on the hydrogen storage behavior. First, the catalytic effect of Ti plays an important role in the improvement of hydrogen storage behavior. The Ti addition enhances the dissociation of hydrogen molecule to hydrogen atom at the surface due to its catalytic effect [36, 37, 39]. Second, the overall affinity for hydrogen increases due to the increase in the (Zr + Ti) combined content, from 69.5 for x = 0 to 73.2 for x = 12 and might lead to an increased number of energetically favorable sites for hydrogen. Thus, it can be said that the combined effect of the above two probable reasons may lead to improved hydrogen storage characteristics of $(Zr_{69.5}Al_{7.5}Cu_{12}Ni_{11})_{100-x}Ti_x$ alloys.

Temperature-programmed desorption (TPD) experiment at heating rate 5°C/min has been done to study the hydrogen desorption behavior of $(Zr_{69.5}Al_{7.5}Cu_{12}Ni_{11})_{100-x}Ti_x$ (x = 0, 4, and 12) quasicrystal-glass composites. The desorption curves of $(Zr_{69.5}Al_{7.5}Cu_{12}Ni_{11})_{100-x}Ti_x$ (x = 0, 4, and 12) alloys are shown in **Figure 9**. The nature of desorption curves for hydrogenated ribbons changed with increasing Ti addition, and this may be attributed to the change in the microstructure of the ribbon with addition of Ti. A small decrease in desorption temperature has been observed at higher Ti content of x = 12. It can be seen from **Figure 9** that full desorption was not observed in the case of $(Zr_{69.5}Al_{7.5}Cu_{12}Ni_{11})_{100-x}Ti_x$ alloys. This behavior is in contrast to stable Ti-based quasicrystal $Ti_{45}Zr_{38}Ni_{17}$, which allows nearly full desorption [22, 40].

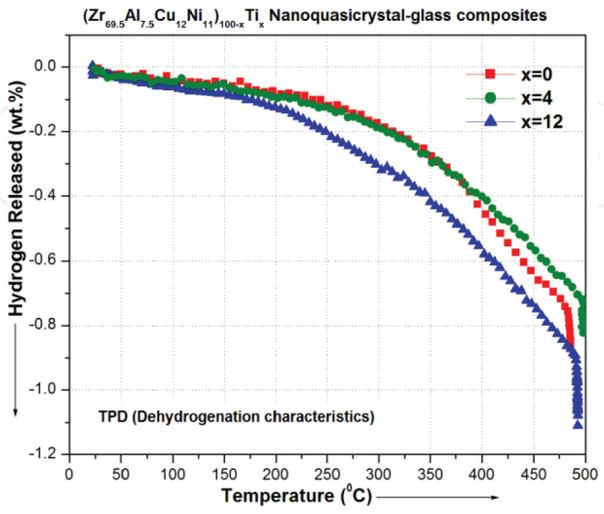

Figure 9. Temperature-programmed desorption (TPD) curves of hydrogenated $(Zr_{69.5}Al_{7.5}Cu_{12}Ni_{11})_{100-x}Ti_x$ (x = 0, 4, and 12) quasicrystal-glass composites (reprinted with kind permission from Ref. [23], Copyright 2013, Elsevier).

http://dx.doi.org/10.5772/66255

3.3. Influence of hydrogenation on the structural and microhardness behavior

In order to investigate the structural changes with hydrogenation, the hydrogenated samples are characterized through XRD. The XRD patterns of the hydrogenated $(Zr_{69.5}Al_{7.5}Cu_{12}Ni_{11})_{100-x}Ti_x$ (x = 0 and 12) ribbons are shown in **Figure 10**. This reveals that I-phase peaks coexist with small concentration of crystalline hydride. This hydride phase has been recognized as ZrH_2 which has a tetragonal lattice with space group: I4/mmm, a = b = 3.519 Å, and c = 4.450 Å. Several earlier studies [15, 16] have reported the formation of such hydride phase on hydrogenation of I-phase in Zr-Al-Cu-Ni alloy. The partial decomposition of I-phase may lead to the formation of hydride phase [15]. During charging from the gas phase, the volume fraction of the quasicrystalline phase exhibits a significant effect on the formation of hydrides [15, 25, 41]. The decrease in the intensity as well as the significant broadening of the I-phase peaks is evident in the XRD patterns for the hydrogenated samples. This is due to the decrease in the size of the grains after hydrogenation. It has been observed that the I-phase peaks are shifted to smaller angle, thus indicating the lattice expansion upon hydrogenation. In the present study, the X-ray diffraction patterns are not only used for the identification of phase transformations with hydrogenation but also used to estimate the quasi-lattice parameters of hydrogenated and partially crystallized ribbons (**Table 3**). The XRD patterns for the hydrogenated ribbons show the formation of crystalline hydride phase along with I-phase. We believe that the volume fraction of crystalline hydride phase is small and the measured hydrogen absorption reflects the amount of hydrogen stored in the quasicrystal.

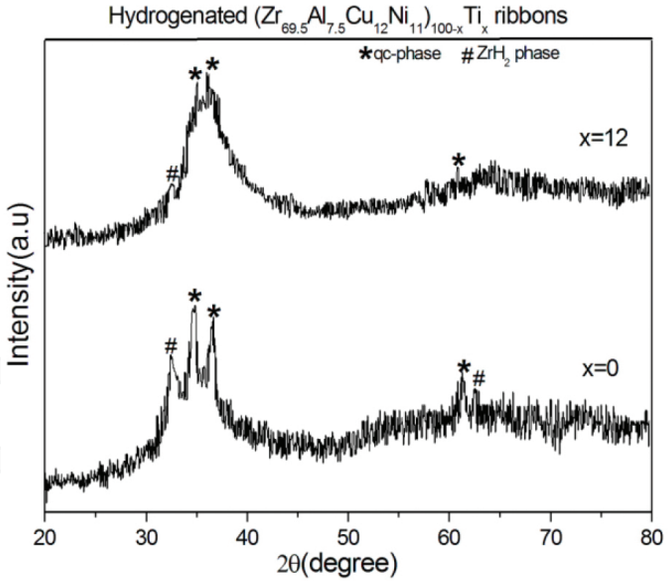

Figure 10. XRD patterns of hydrogenated $(Zr_{69.5}Al_{7.5}Cu_{12}Ni_{11})_{100-x}Ti_x$ (x = 0 and 12) ribbons (reprinted with kind permission from Ref. [23], Copyright 2013, Elsevier).

Here, we also compare the microstructural changes observed after hydrogenation. **Figure 11a** and **b** shows the TEM micrographs of the hydrogenated ribbons with x = 0 and x = 12, respectively. In comparison with **Figure 6a** and **c**, the size of the grains has decreased. The change in the morphology of the quasicrystal grains as well as weakening of the diffraction

spots (marked by arrows in the inset of **Figure 11a**) has been observed for the alloy with x = 0. The weak diffraction spots superimposed on the diffuse halo ring of the amorphous phase can be seen in the SAED pattern for the alloy with x = 12 (inset of **Figure 11b**). These results are in agreement with the results obtained by Zander et al. [41]. It has been observed earlier that even weak hydrogenation may lead to the generation of defects in the icosahedral structure. These defects may be responsible for the diffuseness and domain formation in the microstructure. This would lead to a weakening of the contrast of quasicrystal grains as well as the diffraction spots [17, 41].

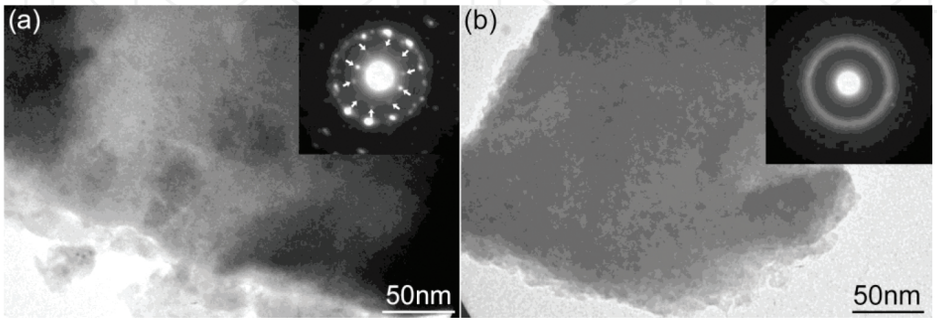

Figure 11. Bright-field TEM micrographs of hydrogenated $(Zr_{69.5}Al_{7.5}Cu_{12}Ni_{11})_{100-x}Ti_x$ ribbons with (a) x = 0 and (b) x = 12 (reprinted with kind permission from Ref. [23], Copyright 2013, Elsevier).

Indentation tests were conducted at room temperature in order to understand the effect of hydrogenation on the microhardness behavior. The SHIMADZU HMV-2T microhardness tester was used under different loads. The standard diamond-pyramid-shaped Vickers indenter with a tip size of ~0.5 μm was used. The hardness (H) was computed in GPa units by employing the following relationship [42–44]:

$$H = 1.854 \times 9.8 \times \frac{P}{d^2} \tag{1}$$

where P is the load (g) and d is the diagonal length in μm. The mean hardness values of at least five loads are reported here with deviations. A notable difference in the indentation behavior of as-synthesized, quasicrystal (qc)-glass composite and hydrogenated qc-glass composite has been observed for the alloys with x = 0, 4, and 12 (c.f. **Figure 12a–c**). Cracks around the indentation impression start to appear when the applied load goes above a certain value. The microhardness tests in the present study were carried out up to this critical load. It can be seen from the hardness versus load characteristic curves that the microhardness tests were carried out up to load of 100 g for the qc-glass composites and 50 g for the hydrogenated qc-glass composites. Hence, load to fracture decreases, and this reveals the decrease in the fracture toughness for the hydrogenated samples. The significant increase in the hardness for the qc-glass composites as compared to as-synthesized ribbons has been observed, and this is due to the precipitation of nano-quasicrystal grains in the amorphous matrix [45–53]. Minor changes in the microhardness behavior after hydrogenation have been observed for the qc-glass

http://dx.doi.org/10.5772/66255

composites. **Table 4** gives hardness values at 50 g of load for the as-synthesized, qc-glass composites, and hydrogenated qc-glass composites. The hardness values of hydrogenated qc-glass composites of x = 0, 4, and 12 at 50 g load are found to be ~7.33 GPa, ~7.57 GPa, and ~7.93 GPa, respectively. These are slightly higher than that of qc-glass composites. The microstructural variation and the partial decomposition of I-phase into crystalline hydride phase during hydrogenation may lead to slight increase in the hardness values. The microhardness might change during hydrogenation by the interstitial content and microstructural changes, e.g., phase transformations as well as precipitations [54–60].

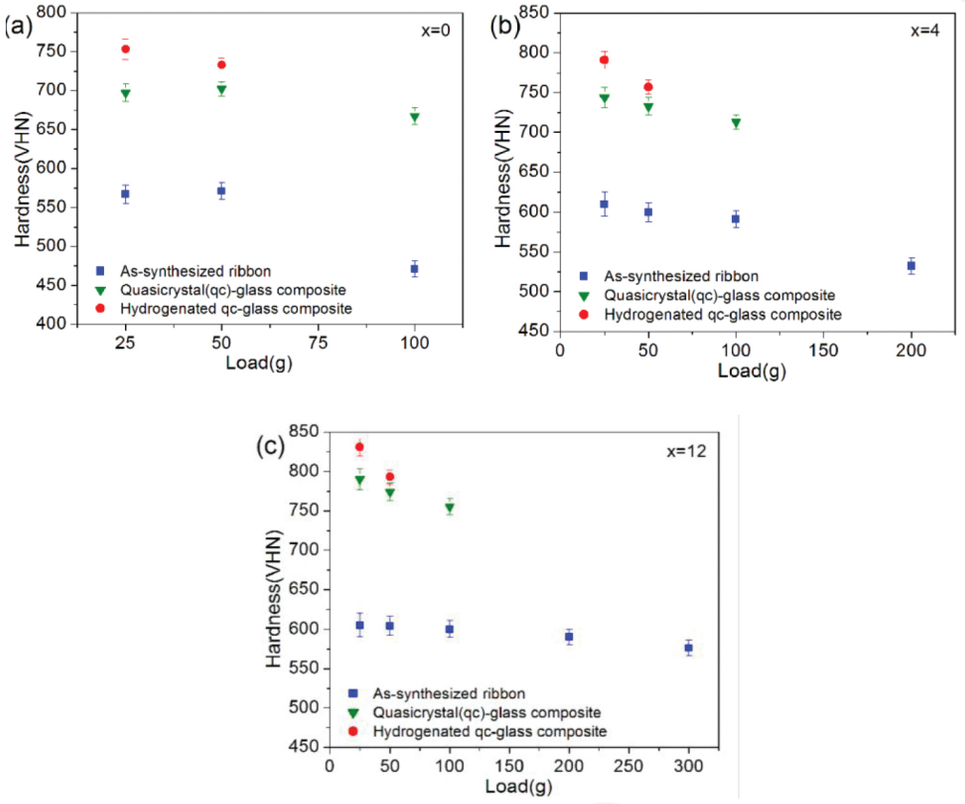

Figure 12. Variation in hardness (VHN) with respect to load for the as-synthesized, quasicrystal(qc)-glass composites, and hydrogenated qc-glass composites (a) x = 0, (b) x = 4, and (c) x = 12 (reprinted with kind permission from Ref. [23], Copyright 2013, Elsevier).

Alloy composition x (at.%)	As-synthesized (±0.10)	Quasicrystal (qc)-glass composite (±0.10)	Hydrogenated qc-glass composite (±0.10)
0	5.71	7.02	7.33
4	6.00	7.33	7.57
12	6.04	7.74	7.93

Table 4. Values of hardness (VHN) (GPa) at 50 g load of as-synthesized, quasicrystal (qc)-glass composites, and hydrogenated qc-glass composites of $(Zr_{69.5}Al_{7.5}Cu_{12}Ni_{11})_{100-x}Ti_x$ alloys (reprinted with kind permission from Ref. [23], Copyright 2013, Elsevier).

4. Conclusion

In this chapter, the hydrogenation behavior of Zr-based quasicrystalline alloy system has been discussed. Based on this study, it may be said that the hydrogen storage capacity of partially quasicrystalline $(Zr_{69.5}Al_{7.5}Cu_{12}Ni_{11})_{100-x}Ti_x$ (x = 0, 4 and 12) alloys has been improved by the addition of Ti. The hydrogen storage capacity is enhanced from ~1.20 wt.% (for x = 0) to ~1.56 wt.% (for x = 12). The enhancement in storage capacity for the alloy with x = 12 is ~23% as compared to the storage capacity of alloy with x = 0. The grain refinement of quasicrystals resulting due to Ti addition has led to the improvement in the hydrogen uptake capacity of $(Zr_{69.5}Al_{7.5}Cu_{12}Ni_{11})_{100-x}Ti_x$ alloys. The microhardness shows only minor changes after hydrogenation of quasicrystal-glass composites. The microstructural and morphological changes affect the hydrogen storage characteristics of quasicrystal-glass composites.

Acknowledgements

One of the authors (Devinder Singh) would like to sincerely acknowledge the financial support from the Department of Science and Technology (DST), New Delhi, India, in the form of INSPIRE Faculty Award [IFA12-PH-39]. Section 3 of this chapter is reproduced with kind permission from Ref. [23] (©2013 Elsevier).

Author details

Devinder Singh[1*], Radhey Shyam Tiwari[2] and Onkar Nath Srivastava[2]

*Address all correspondence to: devinderbhu@yahoo.com

1 Department of Physics, Punjab University, Chandigarh, India

2 Department of Physics, Institute of Science, Banaras Hindu University, Varanasi, India

References

[1] Somekawa H, Watanabe H, Mukai T. Damping properties in Mg-Zn-Y alloy with dispersion of quasicrystal phase particle. Mater Lett 2011;65:3251.

[2] Dubois JM. So useful, those quasicrystals. Isr J Chem 2011;51:1168.

[3] Singh D, Yun Y, Wan W, Grushko B, Hovmöller S, Zou XD. A complex pseudo-decagonal quasicrystal approximant $Al_{37}(Co,Ni)_{15.5}$ solved by the rotation electron diffraction (RED) method. J Appl Crystallogr 2014;47:215.

[4] Hu W, Wang L, Wang L. Quinary icosahedral quasicrystalline Ti–V– Ni–Mn–Cr alloy: a novel anode material for Ni-MH rechargeable batteries. Mater Lett 2011;65:2868.

[5] Singh D, Yun Y, Wan W, Grushko B, Hovmöller S, Zou XD. Structure determination of a pseudo-decagonal quasicrystal approximant by the strong-reflections approach and rotation electron diffraction. J Appl Crystallogr 2016;49:433–441 doi: 10.1107/S1600576716000042.

[6] Yadav TP, Singh D, Shahi RR, Shaz MA, Tiwari RS, Srivastava ON. Formation of quasicrystalline phase in $Al_{70-x}Ga_xPd_{17}Mn_{13}$ alloys. Philos Mag 2011;91:2474.

[7] Yadav TP, Singh D, Shaz MA, Tiwari RS, Srivastava ON. Synthesis of quasicrystalline film of Al-Ga-Pd-Mn alloy. Thin Solid Films 2013;534:265.

[8] Kelton KF, Kim WJ, Stroudb RM. A stable Ti-based quasicrystal. Appl Phys Lett 1997;70:24.

[9] Stroud RM, Viano AM, Gibbons PC, Kelton KF. Stable Ti-based quasicrystal offers prospect for improved hydrogen storage. Appl Phy Lett 1996;69:20.

[10] Takasaki A, Kelton KF. Hydrogen storage in Ti-based quasicrystal powders produced by mechanical alloying. Int J Hydrogen Energy 2006;31:183.

[11] Hudson MSL, Dubey PK, Pukazhselvan D, Pandey SK, Singh RK, Raghubanshi H, et al. Hydrogen energy in changing environmental scenario: Indian context. Int J Hydrogen Energy 2009;34:7358.

[12] Lototsky MV, Yartys VA, Zavaliy IY. Vanadium-based BCC alloys: phase-structural characteristics and hydrogen sorption properties. J Alloys Compds 2005;404:421.

[13] Sakintuna B, Lamari D, Hirscher M. Metal hydride materials for solid hydrogen storage: a review. Inter J Hydrogen Energy 2007;32:1121.

[14] Rud AD, Schmidt U, Zclinska GM, Lakhnik AM, Kolbasov GY, Danilov MO. Atomic structure and hydrogen storage properties of amorphous–quasicrystalline Zr–Cu–Ni–Al melt-spun ribbons. J Non Cryst Solids 2007;353:3434.

[15] Huett VT, Zander D, Jastrow L, Majzoub EH, Kelton KF, Köster U. Gaseous hydrogen charging of Zr–Cu–Ni–Al glasses and quasicrystals. J Alloys Compds 2004;379:16.

[16] Zander D, Tal-Gutelmacher E, Jastrow L, Köster U, Eliezer D. Hydrogenation of Pd-coated Zr–Cu–Ni–Al metallic glasses and quasicrystals. J Alloys Compds 2003;356-357:654.

[17] Apih T, Khare V, Klanjsek M, Jeglic P, Dolinsek J. Hydrogen diffusion in partially quasicrystalline Zr69.5Cu12Ni11Al7.5. Phys Rev B 2003;68:212202.

[18] Eliaz N, Eliezer D, Abramov E, Zander D, Köster U. Hydrogen evolution from Zr-based amorphous and quasicrystalline alloys. J Alloys Compds 2000;305:272.

[19] Köster U, Zander D, Meinhardt J, Eliaz N, Eliezer D. Hydrogen in quasicrystalline Zr-Cu-Ni-Al, in: Takeuchi S, Fujiwara T (Eds), Proceedings of the Sixth International Conference on Quasicrystals, Tokyo, 1997, World Scientific, Singapore, 1998, p. 313.

[20] Ismail N, EI-Meligi AA, Uhlemann M, Gebert A, Eckert J, Schultz L. Hydrogenation of Zr–Cu–Al–Ni–Pd metallic glasses by electrochemical means. J Alloys Compds 2009;480:321.

[21] Köster U, Zander D, Leptien H, Eliaz N, Eliezer D. Hydrogenation and crystallization of Zr-Cu-Ni-Al metallic glasses, in: Johnson WL, Inoue A, Liu AT, (Eds), Proceedings of the MRS-Symposium on Bulk Metallic Glasses, Boston, 1998. Mater Res Soc Symp Proc, vol 554, Pittsburgh, 1999: p. 287.

[22] Shahi RR, Yadav TP, Shaz MA, Srivastava ON, Smaalen Van S. Effect of processing parameter on hydrogen storage characteristics of as quenched $Ti_{45}Zr_{38}Ni_{17}$ quasicrystalline alloys. Int J Hydrogen Energy 2011;36:592.

[23] Singh D, Shahi RR, Yadav TP, Mandal RK, Tiwari RS, Srivastava ON. Hydrogenation of $(Zr_{69.5}Al_{7.5}Cu_{12}Ni_{11})_{100-x}Ti_x$ quasicrystalline alloys and its effect on their structural and microhardness behaviour. J Non-Cryst Solids. 2013;380:11.

[24] Huang H, Li R, Yin C, Zheng S, Zhang P. Hydrogenation study of suction-cast $Ti_{40}Zr_{40}Ni_{20}$ quasicrystal. Int J Hydrogen Energy 2008;33:4607.

[25] Zander D, Köster U, Eliaz N, Eliezer D. Influence of hydrogen on formation and stability of Zr-based quasicrystals. Mater Sci Eng 2000;294-296:112.

[26] Sinning HR, Scarfone R, Golovin JS. Mechanical spectroscopy of hydrogen-absorbing quasicrystals. Mater Sci Eng A 2004;370:78.

[27] Wang YM. Structure evolution of Zr-based Glass-Forming Alloys and Composition Design Methodology for Good Glass-Forming Abilities, Ph.D. thesis, City University of Hong Kong, Hong Kong (2007).

[28] Kühn U, Eymann K, Mattern N, Eckert J, Gebert A, Bartusch B, Schultz L. Limited quasicrystalformationinZr–Ti–Cu–Ni–Albulkmetallicglasses. ActaMater2006;54:4685.

[29] Singh D, Tiwari RS, Srivastava ON, Mandal RK. Synthesis and Mechanical Properties of $Zr_{69.5}Ga_{7.5}Cu_{12}Ni_{11}$ Metallic Glass and Nanoquasicrystal-Glass Composites. Emerging Paradigms in Nanotechnology. Pearson Education, Chennai, India. 2013;81: ISBN: 978-81-317-8991-9.

[30] Singh D, Mandal RK, Tiwari RS, Srivastava ON. Role of Nano-Quasicrystals in the Formation of Shear Bands in Zr-based Glassy Alloys. Nanotechnology: Novel Perspectives and Prospects. McGraw-Hill, USA. 2015; ISBN: 978-93-392-2109-6.

[31] Singh D, Tiwari RS, Srivastava ON. Metallic Glasses, Quasicrystals and their Nanocomposites. Lap Lambert Academic Publishing, Germany. 2014;111156:165. ISBN: 978-3-659-62088-1.

[32] Hong E, Dunand DC, Choe H. Hydrogen-induced transformation superplasticity in zirconium. Int J Hydrogen Energy 2010;35:5708.

[33] Singh D, Yadav TP, Mandal RK, Tiwari RS, Srivastava ON. Effect of Ga substitution on the crystallization behaviour and glass forming ability of Zr–Al–Cu–Ni alloys. Mater Sci Eng A 2010;527:469.

[34] Zander D, Leptian H, Köster U, Eliaz N, Eliezer D. Hydrogenation of Zr-based metallic glasses and quasicrystals. J Non-Cryst Solids 1999;250-252:893.

[35] Singh D, Yadav TP, Mandal RK, Tiwari RS, Srivastava ON. Effect of Ti addition on the quasicrystalline phase formation and indentation characteristics of $Zr_{69.5}Al_{7.5}Cu_{12}Ni_{11}$ alloy. Philos Mag 2011;91:2837.

[36] Bancel PA, Heiney PA, Stephans PW, Goldmann AI, Horn PM. Structure of rapidly quenched Al-Mn. Phys Rev Lett 1985;54:2422.

[37] Saida J, Matsushita M, Li C, Inoue A. Effects of Ag and Pd on the nucleation and growth of the nano-icosahedral phase in $Zr_{65}Al_{7.5}Ni_{10}Cu_{7.5}M_{10}$ (M = Ag or Pd) metallic glasses. Philos Mag Lett 2000;80:737.

[38] Wu Y, Lototsky MV, Solberg JK, Yartys VA, Han W, Zhou SX. Microstructure and novel hydrogen storage properties of melt-spun Mg–Ni–Mm alloys. J Alloys Compds 2003;477:262.

[39] Qiang JB, Zhang W, Xie GQ, Inoue A. Effect of Ti addition on the crystallization behavior and glass-forming ability of Zr–Al–Cu alloys. J Non-Cryst Solids 2008;354:2054.

[40] Viano AM, Majzoub EH, Stroud RM, Kramer MJ, Misture ST, Gibbons PC, Kelton KF. Hydrogen absorption and storage in quasicrystalline and related Ti-Zr-Ni alloys. Philos Mag A 1998;78:131.

[41] Zander D, Köster U, Khare V. Hydrogen induced transformations in Zr–Cu–Ni–Al quasicrystals. J Non-Cryst Solids 2004;334–335:247.

[42] Mukhopadhyay NK, Weatherly GC, Embury JD. An analysis of microhardness of single-quasicrystals in the Al–Cu–Co–Si system. Mater Sci Eng A 2001;315:202.

[43] Singh D, Mandal RK, Tiwari RS, Srivastava ON. Effect of cooling rate on the crystallization and mechanical behaviour of Zr-Ga-Cu-Ni metallic glass composition. J Alloys Compds 2015;648:456.

[44] Singh D, Singh D, Yadav TP, Mandal RK, Tiwari RS, Srivastava ON. Synthesis and indentation behaviour of amorphous and nanocrystalline phases in rapidly quenched Cu-Ga-Mg-Ti and Cu-Al-Mg-Ti alloys. Metallogr Microstruct Anal 2013;2:321.

[45] Singh D, Yadav TP, Mandal RK, Tiwari RS, Srivastava ON. Indentation characteristics of metallic glass and nanoquasicrystal-glass composite in Zr–Al (Ga)–Cu–Ni alloys. Intermetallics 2010;18:2445.

[46] Singh D, Mandal RK, Tiwari RS, Srivastava ON. Nanoindentation characteristics of Zr $_{69.5}Al_{7.5-x}Ga_xCu_{12}Ni_{11}$ glasses and their nanocomposites. J Alloys Compds 2011;509:8657.

[47] Yadav TP, Singh D, Tiwari RS, Srivastava ON. Enhanced microhardness of mechanically activated carbon–quasicrystal composite. Mater Lett 2012;80:5.

[48] Singh D, Singh Manjeet, Yadav TP, Mandal RK, Tiwari RS, Srivastava ON. Nanoindentation studies of metallic glasses and nanoquasicrystal–glass composites in Zr–Al (Ga)–Cu–Ni alloys. Inter J Nanosci 2011;10:929.

[49] Singh D, Yadav TP, Tiwari RS, Srivastava ON. Phase formation in rapidly quenched Cu-based alloys. J Mater Sci 2009;44:3883.

[50] Singh D, Singh D, Mandal RK, Srivastava ON, Tiwari RS. Glass forming ability, thermal stability and indentation characteristics in $Ce_{75}Al_{25-x}Ga_x$ metallic glasses. J Alloys Compds 2014;590:15.

[51] Singh D, Singh D, Srivastava ON, Tiwari RS. Microstructural effect on the low temperature transport properties of Ce-Al (Ga) metallic glasses. Scripta Mater. 2016;118:24.

[52] Singh D, Singh D, Mandal RK, Srivastava ON, Tiwari RS. Crystallization behaviour and mechanical properties of $(Al_{90}Fe_5Ce_5)_{100-x}Ti_x$ amorphous alloys. J Alloys Compds 2016;687:990.

[53] Singh D, Singh D, Mandal RK, Srivastava ON, Tiwari RS. Effect of annealing on the devitrification behaviour and mechanical properties of rapidly quenched Ce-based glassy alloys. J Non-Cryst Solids 2016;445:53.

[54] Jayalakshmi S, Kim KB, Fleury E. Effect of hydrogenation on the structural, thermal and mechanical properties of Zr_{50}–Ni_{27}–Nb_{18}–Co_5 amorphous alloy. J Alloys Compds 2006;417:195.

[55] Yamaura SI, Hasegawa M, Kimura H, Inoue A. Effects of hydrogen on the mechanical properties of $Ti_{50}Ni_{25}Cu_{25}$ metallic glass. Mater Trans 2002;43:2543.

[56] Zander D, Olson DL, Eliezer D. Mutual effects of hydrogenation and deformation in Ti-Nb alloys. Metall Mater Trans A 2003;34A:2199.

[57] Jayalakshmi S, Ahn JP, Kim KB, Fleury E. Hydrogen-induced amorphization and embrittlement resistance in Ti-based in situ composite with bcc-phase in an amorphous matrix. J Mater Res 2007;22:428.

[58] Jayalakshmi S, Fleury E, Lee DY, Chang HJ, Kim DH. Hydrogenation of $Ti_{50}Zr_{25}Co_{25}$ amorphous ribbons and its effect on their structural and mechanical properties. Philos Mag Lett 2008;88:303.

[59] Singh D, Mandal RK, Tiwari RS, Srivastava ON. Mechanical Behavior of Zr-Based Metallic Glasses and Their Nanocomposites, Metallic Glasses - Formation and Properties, Dr. Behrooz M (Ed.), InTech, Rijeka, Croatia – European union. 2016, doi: 10.5772/64221.

[60] Mandal RK, Tiwari RS, Singh D, Singh D. Influence of Ga substitution on the mechanical behavior of $Zr_{69.5}Al_{7.5-x}Ga_xCu_{12}Ni_{11}$ and $Ce_{75}Al_{25-x}Ga_x$ metallic glass compositions. MRS Proceeding. 2015;1757. doi: 10.1557/opl.2015.45.

IntechOpen